Cerebral Cortex, January 2016;26: 427–439

doi: 10.1093/cercor/bhv232
Advance Access Publication Date: 15 October 2015
Original Article

ORIGINAL ARTICLE

Nogo Receptor Signaling Restricts Adult Neural Plasticity by Limiting Synaptic AMPA Receptor Delivery

Susumu Jitsuki[1,†], Waki Nakajima[1,†], Kiwamu Takemoto[1,2], Akane Sano[1], Hirobumi Tada[1], Aoi Takahashi-Jitsuki[1] and Takuya Takahashi[1]

[1]Department of Physiology, Yokohama City University Graduate School of Medicine, Yokohama 236-0004, Japan and [2]JST, PRESTO, Saitama 332-0012, Japan

Address correspondence to Takuya Takahashi. Email: takahast@yokohama-cu.ac.jp

[†]S.J. and W.N. contributed equally to this work.

Abstract

Experience-dependent plasticity is limited in the adult brain, and its molecular and cellular mechanisms are poorly understood. Removal of the myelin-inhibiting signaling protein, Nogo receptor (NgR1), restores adult neural plasticity. Here we found that, in NgR1-deficient mice, whisker experience-driven synaptic α-amino-3-hydroxy-5-methyl-4-isoxazole propionic acid receptor (AMPAR) insertion in the barrel cortex, which is normally complete by 2 weeks after birth, lasts into adulthood. In vivo live imaging by two-photon microscopy revealed more AMPAR on the surface of spines in the adult barrel cortex of NgR1-deficient than on those of wild-type (WT) mice. Furthermore, we observed that whisker stimulation produced new spines in the adult barrel cortex of mutant but not WT mice, and that the newly synthesized spines contained surface AMPAR. These results suggest that Nogo signaling limits plasticity by restricting synaptic AMPAR delivery in coordination with anatomical plasticity.

Introduction

Experience-driven neural plasticity shapes neural circuits during brain development, but declines after an early postnatal critical period, and only limited plasticity remains in the adult brain (Issa et al. 1999; Grutzendler et al. 2002; Morishita and Hensch 2008; Feldman 2009; Holtmaat and Svoboda 2009; Bavelier et al. 2010). This restricted plasticity limits functional recovery after central nervous system damage in adulthood. Thus, elucidating the molecular and cellular mechanisms that restrict adult plasticity could lead to new therapies to promote functional recovery from damage to the adult central nervous system.

Some molecules are known to limit adult neural plasticity, such as the myelin-inhibiting signaling proteins Nogo receptor (Nogor1/Rtn4r:NgR) and PirB, and the modulator of nicotinic acetylcholine receptor (Lynx1) (McGee et al. 2005; Syken et al. 2006; Atwal et al. 2008; Morishita et al. 2010). However, the mechanisms by which these molecules prevent adult neural plasticity are unknown. Nogo was first identified as an inhibitor of axonal growth and regeneration (Bregman et al. 1995; Chen et al. 2000; GrandPre et al. 2000; Prinjha et al. 2000; Fournier et al. 2001; Kim et al. 2003; Zheng et al. 2003). In NgR1-deficient mice, the duration of ocular dominance plasticity in the visual cortex, which normally ends at postnatal day (P) 32, extends into adulthood (McGee et al. 2005). Furthermore, spine turnover is increased in the adult cortex of NgR1 mutant mice (Akbik et al. 2013). These reports indicate that NgR signaling restricts experience-dependent plasticity in the adult brain.

Excitatory glutamatergic synapses play central roles in cognitive function (Zamanillo et al. 1999; Ungless et al. 2001; Lee et al. 2003; Whitlock et al. 2006; Matsuo et al. 2008; Ryu et al. 2008; Wright et al. 2008; Dachtler et al. 2011). Sensory experience drives the transport of the α-amino-3-hydroxy-5-methyl-4-isoxazole propionic acid (AMPA) receptor (AMPAR), one of the glutamate receptors, into synapses and contributes to neural-circuit establishment in young animals (Takahashi et al. 2003; Rumpel et al.

2005; Clem and Barth 2006; Kessels and Malinow 2009; Makino and Malinow 2011; Mitsushima et al. 2011; Miyazaki, Kunii, et al. 2012; Miyazaki et al. 2013). In rats at ages P12–P14, natural whisker experience drives AMPAR into synapses onto pyramidal neurons formed from layer 4 to 2/3 of the developing barrel cortex; however, in P21–P23 rats, this incorporation of AMPAR no longer occurs, indicating that a critical period exists for the sensory experience-driven synaptic trafficking of AMPAR (Jitsuki et al. 2011).

Here we report that the natural whisker experience-driven incorporation of AMPAR into synapses onto pyramidal neurons in layer 4–2/3 in the barrel cortex continues into adulthood in NgR1-deficient mice. In vivo live imaging with a two-photon microscope revealed more AMPAR on the surface of spines in the adult barrel cortex of NgR1-deficient than wild-type (WT) mice. Trimming the whiskers of adult NgR1-deficient mice decreased the amount of surface AMPAR at spines to that of WT mice with intact whiskers. We found that 2 h of whisker stimulation also produced new spines in the adult barrel cortex of mutant but not WT mice, and the newly synthesized spines contained surface AMPAR, indicating the functional contribution of these spines. These results suggest that Nogo signaling limits plasticity by restricting synaptic AMPAR delivery in coordination with anatomical plasticity.

Materials and Methods

Ethics Statement

All experiments were conducted according to the Guide for the Care and Use of Laboratory Animals (Japan Neuroscience Society) and the Guide for Yokohama City University. All animal experiments were approved by the Animal Care and Use Committee of Yokohama City University (authorization number: F-A-14-024). All surgical procedures were performed under anesthesia, and every effort was made to minimize suffering.

Animals

Male c57BL6/J mice and NgR1-knockout mice (Kim et al. 2004; McGee et al. 2005) (P12–P14, 3 months old) were housed on a 12-h light/dark cycle with ad libitum access to water and food. Procedures were performed in strict compliance with the animal use and care guidelines of Yokohama City University. Male c57BL6/J mice were used as control animals. The NgR1-knockout mice were kindly provided by Dr Stephen Strittmatter. The AMPA/N-methyl-D-aspartate (NMDA) (A/N) ratio and in vivo imaging in intact animals were examined by investigators blinded to genotype.

DNA Constructs

The GFP-tagged GluA1 (GFP-GluA1) and Herpes virus constructs were prepared as previously described (Shi et al. 2001; Jitsuki et al. 2011). For the expression of NgR1 (*Rtn4r*, Gene ID: 65079) and the dominant-negative form of cofilin (cofilin S3E), the NgR1 or cofilin S3E was subcloned into the CSII-EF-MCS-IRES-VENUS vector (kindly provided by Drs Hiroyuki Miyoshi and Atsushi Miyawaki) using Not1. The NgR1-IRES2-Venus or cofilin S3E-IRES2-Venus was subcloned into the pHSVPrPUC vector using EcoR1 and confirmed by sequencing. The cofilin S3E construct was kindly provided by Dr James Zheng, and the NgR1 construct was kindly provided by Dr Stephen Strittmatter. The pCALNL-SEP-GluA1 and pCAG-$ER^{T2}CreER^{T2}$ constructs, kindly provided by Dr Roberto Malinow (Makino and Malinow 2011), and the tdTomato were subcloned into pEF-Bos for in utero electroporation. All short hairpin constructs were generated using the pLenti-Lox 3.7 vector. The pLenti-Lox 3.7, pLenti-Lox 3.7-shNgR1, and pLenti-Lox 3.7-shTROY were kindly provided by Dr Michael Greenberg (Wills et al. 2012). The CMV promoter of pLenti-Lox 3.7 was replaced with the CaMKII promoter using Not1/Nhe1. The following oligonucleotides were annealed with their complimentary sequence and inserted into the Hpa1 sites of pLenti-Lox3.7: scrambled NgR1 (SCRNgR1) TGCA TTCTCTAAGCCAACG, scrambled TROY (SCRTROY) CTAGAAGTGTT CCAAGTGG. ShRNA-resistant NgR (res-NgR) or Troy (res-Troy) constructs were generated by mutating the ShRNA target at 4 or 5 different nucleotides without changing the amino acid sequence. ShRNA-resistant constructs were synthesized by Eurofins Genomics K.K. (Tokyo, Japan). For lentiviral expression, ShRNA-resistant constructs were subcloned into the CSII-EF-MCS-IRES2-hKO1 vector (kindly provided by Dr Hiroyuki Miyoshi, RIKEN, Tsukuba, Japan). All constructs were confirmed by DNA sequencing.

Electrophysiology

Mice were anesthetized with an isoflurane–oxygen mixture, and the brain was removed. The brain was quickly transferred into gassed (95% O_2 and 5% CO_2) ice-cold dissection buffer as described previously (Jitsuki et al. 2011). Coronal brain slices were cut (350 μm, Leica VT1000) in dissection buffer. The slices were then incubated in artificial cerebrospinal fluid (ACSF) containing 118 mM NaCl, 2.5 mM KCl, 4 mM $CaCl_2$, 4 mM $MgCl_2$, 26 mM $NaHCO_3$, 1 mM NaH_2PO_4, 10 mM glucose (Miyazaki, Takase, et al. 2012). Patch recording pipettes (3–7 MΩ) were filled with intracellular solution as described previously (Jitsuki et al. 2011; Mitsushima et al. 2013; Tada et al. 2013).

For rectification experiments, the recording chamber was perfused with ACSF containing 0.1 mM picrotoxin, 4 μM 2-chloroadenosine, and 0.1 mM D,L-aminophosphonovaleric acid (APV) at 22–25–°C. Whole-cell recordings were obtained from infected or uninfected layer 2/3 pyramidal neurons of the mouse barrel cortex with a Multiclamp 700B (Axon Instruments). Bipolar tungsten stimulating electrodes were placed in layer 4. The stimulus intensity was increased until a synaptic response of amplitude greater than approximately 10 pA was recorded. Synaptic AMPAR-mediated currents at –60 mV and +40 mV were averaged over 30–50 trials, and their ratio was used as an index of rectification (Hayashi et al. 2000).

AMPA/NMDA ratios were calculated as the ratio of the peak current at –60 mV to the current at +40 mV 50 ms after stimulus onset (40–50 traces averaged for each holding potential), without D,L-APV in the recording chamber. To avoid stimulating the same sets of synapses when recording from distinct neurons, we picked up neurons from different barrel columns. LTP was induced by pairing 5-Hz stimulation with depolarization of the postsynaptic neuron to +0 mV for 90 s. Recordings were maintained for at least 40 min after pairing. The excitatory postsynaptic current (EPSC) amplitude throughout the recording was always normalized to the average baseline amplitude before pairing. Experiments were excluded from analysis if unpaired control pathways displayed changes in transmission.

For recording of lateral input, stimulating electrodes were placed in layer 2/3 of adjacent side approximately 200–300 m away from the recorded cells. NMDA receptor-mediated EPSCs were recorded at +40 mV, while perfusing with ACSF containing 0.1 mM picrotoxin, 4 μM 2-chloroadenosine, and 20 μM CNQX. Paired-pulse ratio (second/first EPSC amplitude) was measured using 2-paired stimuli with an interval of 30 ms. Data were analyzed using Clampfit10.2 (Molecular Devices).

In vivo Infection of Neocortical Neurons

Mice were deeply anesthetized with an isoflurane–oxygen mixture. The skin overlying the skull was cut and gently pushed to

the side. The anterior fontanel was identified, and a region 1-mm posterior, 3.5-mm lateral was gently pierced with a dental drill. Recombinant Herpes virus or Lentivirus was pressure-injected through a pulled-glass capillary (Narishige) into the barrel cortex. After injection, the skin was repositioned and maintained with cyanoacrylate glue. Mice were kept on a heating pad during the procedures, and returned to their home cages after regaining movement.

In Utero Electroporation

Layer 2/3 progenitor cells were transfected by in utero electroporation. E15 timed pregnant mice were anesthetized with an isoflurane–oxygen mixture. Approximately 1 μL of DNA solution containing Fast Green was pressure injected by mouth through a pulled-glass capillary tube (Narishige) into the right lateral ventricle of each embryo. The head of each embryo was placed between tweezer-type electrodes with the anode contacting the right hemisphere. Electroporation was achieved with five square pulses (duration = 50 ms, frequency = 1 Hz, voltage = 35 V; Bex Co.).

Cre Recombinase Activation by 4-OHT

4-OHT (Sigma-Aldrich) was dissolved in ethanol at 20 mg/mL and diluted with 9 volumes of sesame oil (Sigma-Aldrich). Diluted 4-OHT (2 mg/mL) was intramuscularly injected into mice 2 days before imaging or electrophysiology.

Surgery

Imaging windows were installed above the barrel cortex in mice about 2 months old. Mice were deeply anesthetized with an isoflurane–oxygen mixture. A craniotomy (1.5-mm diameter) was opened above the right barrel cortex (1 mm posterior from bregma; 3.5 mm lateral from midline), leaving the dura intact. The dura was covered with 1.8% agarose (Type-IIIA, Sigma) dissolved in cortex buffer (Holtmaat and Svoboda 2009), and covered with a 5-mm custom-made coverslip (Matsunami Glass) that was sealed into place with dental cement. A custom-designed head-mounting apparatus was attached to the animal's skull to reduce motion-induced artifacts during imaging. For a subset of animals, the position of the imaging window was mapped relative to the layer 4 barrels using standard histological methods.

In vivo Imaging

Animals were anesthetized intraperitoneally with 100 mg/kg ketamine/10 mg/kg xylazine or 1.25 mg/kg urethane (for artificial whisker stimulation) and mounted on the microscope. Images were collected using a 2-photon laser-scanning microscope (FV-1000MPE; Olympus) with a water immersion objective (×25 1.05 NA; Olympus) and an imaging depth of 100 μm from the surface to 200 μm into the barrel cortex, and the z-stack step size was set to 0.5 μm. SEP and tdTomato were excited at 910 nm with a Ti:sapphire laser (Mai Tai DeepSee; Spectra-Physics). Green and red fluorescent signals were separated by a set of dichroic mirrors and filters (Olympus). SEP and tdTomato fluorescence in spines and dendrites was measured as integrated green and red fluorescence, respectively, after background and leak subtraction. The ratio of SEP fluorescence intensity of the spine head to dendritic shaft was measured on manually selected spine head and dendritic-shaft areas. At least 20 spines per animal were selected. Pseudo-color ratiometric heat maps were generated using MATLAB software (MathWorks).

Artificial Stimulation of Mouse Whiskers

After in vivo imaging, the whiskers of the mice were stimulated by a motor-driven rotating stick (Mabuchi motor RE-240RA-2670) for 2 h. Mice were anesthetized with 1.25 mg/kg urethane and kept on a heating pad during the procedures. After whisker stimulation, in vivo imaging was resumed.

Preparation of Brain Lysate

Mouse brains were rapidly dissected and sliced to a 2-mm thickness in a Rodent Brain Matrix (ASI Instruments). Sections corresponding to Figure 29–47 in Franklin & Paxinos MOUSE BRAIN 3rd edition (Franklin and Paxinos 2007) were selected, and the Somatosensory cortex including barrel cortex was excised 2–5 mm from the midline along with corpus callosum. The sample was then stored in liquid nitrogen. Synaptoneurosome fractions were prepared as previously described (Miyazaki, Takase, et al. 2012). Frozen samples were homogenized in ice-cold homogenization buffer A (10 mM Hepes, 1.0 mM EDTA, 2.0 mM EGTA, 0.5 mM DTT, 0.1 mM PMSF, 10 mg/liter leupeptin, 100 nM microcystin). Tissue was homogenized in a glass/glass tissue homogenizer. Homogenates were passed through two 100-μm-pore nylon mesh filters, and then through a 5-μm-pore filter. Filtered homogenates were centrifuged at 3600 × *g* for 10 min at 4°C. The resultant pellets were resuspended in 100 μL boiling 1% SDS, boiled for 10 min, and stored at –80°C.

To prepare the crude lysates, frozen samples were homogenized in ice-cold homogenization buffer B (150 mM NaCl, 20 mM HEPES, 4 mM EDTA, 1 mM EGTA, and 1% Triton X-100, with a protease inhibitor tablet and phosphatase inhibitor cocktail) using a glass/glass tissue homogenizer. Lysates were sonicated and centrifuged at 15 000 × *g* for 15 min at 4°C. Supernatant fractions were boiled in homogenization buffer B for 5 min at 100°C.

To compare the relative content of pCofilin or Cofilin in synaptoneurosomes, each sample from a single animal was homogenized in ice-cold homogenization buffer A, and the homogenates were divided into 2 aliquots. Aliquot 1 was used as the synaptoneurosome fraction. Aliquot 2 was used as the crude lysate. The amounts of pCofilin and Cofilin in aliquot 1 and aliquot 2 were compared using following Western blot analysis.

Cortical Culture

Cortical neurons derived from the E16 brains of c57BL6/J mice were plated at a density of 2.5–4 × 10^4 cells/well in 6-well dishes (Greiner Japan) that were coated with poly-L-lysine and grown in neurobasal medium (Life Technologies) supplemented with B27 (Gibco) and GlutaMAX (Gibco). At 7 days in vitro (Div), shNgR1 or shTROY was introduced by lentivirus-mediated gene transfer. Cortical neurons were harvested with homogenization buffer at 7 days after lentiviral infection. Homogenates were subjected to western blot analysis.

Immunoprecipitation

To analyze the ubiquitination of GluA1, samples of barrel cortex were collected and homogenized in lysis buffer (150 mM NaCl, 20 mM HEPES, 4 mM EDTA, 1 mM EGTA, and 1% Triton X-100, with a protease inhibitor tablet and phosphatase inhibitor cocktail) using a tissue homogenizer. Lysates were sonicated and centrifuged at 15 000 × *g* for 15 min at 4°C. Supernatant fractions were incubated with an anti-GluA1 antibody (1 μg, Millipore; clone C3T) overnight at 4°C, followed by incubation with 20 μL protein G Mag Sepharose (GE Healthcare) for 1 h at 4°C. Immunoprecipitates were

washed 3 times with lysis buffer, and then boiled in SDS buffer for 5 min at 100°C.

Western Blotting

Samples were processed using 10% acrylamide gels and transferred to PVDF membranes. Membranes were blocked with 1% blocking buffer (Perfect-block; MoBiTec) in TBS-TritonX (0.1%) for 1 h and incubated overnight with a primary antibody against Nogo-A 1 : 1000 (Millipore), MAG 1:1000 (Cell Signaling Technology), OMgp 1:4000 (Millipore), Troy 1:500 (R&D Systems), NgR 1:1000 (R&D Systems), phospho-S3cofilin 1:1000 (Abcam: ab12866), cofilin 1:1000 (Abcam: ab42824), GluA1 1:1000 (Millipore; clone C3T), NEDD4 1:4000 (Abcam; ab14592), phospho-S845GluA1 1:1000 (Millipore), phospho-S831GluA1 1:1000 (Millipore), β-actin 1:2000 (Sigma), GAPDH 1:2000 (Cell Signaling Technology), or Ubiquitin 1:200 (Santa Cruz: sc8017) at 4°C. Blots were then washed in TBS-TritonX and placed in HRP-conjugated anti-rabbit or anti-mouse secondary antibody at a 1:1000 dilution. Blots were then washed and reacted with electrochemiluminescence (ECL) or ECL-prime reagents. ECL-treated blots were quantified by densitometry using LAS4000 (Fujifilm). Protein phosphorylation data are expressed as percentages of the control.

Golgi Staining

Brain samples of adult WT and NgR1-deficient mice were removed and submerged into Golgi-Cox solution (FD NeuroTechnologies). The frozen tissue was sectioned at 200 μm on a microtome, followed by staining according to the manufacturer's procedures. For the morphometric analysis, the basal dendrites of pyramidal neurons were randomly selected from layer 2/3 of the barrel cortex. Only neurons that showed no breaks in the staining along the dendrites were analyzed. Images were acquired using a light microscope at ×120 magnification (BZ-9000; Keyence), and measurement was performed at least 40 μm away from the soma, on secondary and tertiary branches. Dendritic spines were assigned to the morphological category (Harris et al. 1992; Lee et al. 2008) that most resembled the shape of the spine. Spine density was calculated by dividing the number of spines on a segment by the length of the segment and was expressed as the number of spines per 10 μm of dendritic length.

Statistics

All data are presented as mean ± SEM. All statistics were analyzed using SPSS software (SPSS 22.0; IBM). Data were analyzed by Student's *t*-test, one-way ANOVA, 2-way ANOVA with repeated measures. When comparing more than 2 groups, ANOVA followed by post hoc Bonferroni analyses or Fisher's Least Significant Difference was used. $P < 0.05$ was considered statistically significant. Statistical analyses were performed based on the number of animals.

Results

Natural Whisker Experience Does not Drive AMPAR Into Synapses in the Adult Barrel Cortex

To examine the natural sensory experience-driven synaptic AMPAR delivery in the barrel cortex, we first measured the ratio of AMPAR-mediated synaptic transmission to NMDA receptor (NMDAR)-mediated synaptic current (A/N ratio) in mice. As reported in rats (Takahashi et al. 2003), a larger A/N ratio was detected in mice with intact whiskers than in P14 mice deprived of whisker input ("whisker deprived") from P12, indicating that whisker experience actively drives AMPAR into synapses at this age (Fig 1*A*). However, no difference in the A/N ratio was observed between 3-month-old intact and whisker-deprived mice (deprivation for 2 days before recordings), suggesting that adults lack whisker experience-driven synaptic AMPAR delivery (Fig 1*B*). No difference in the decay or input–output curve of NMDAR-mediated synaptic responses was observed between intact and whisker-deprived animals at P14 or adulthood (see Supplementary Fig 1), supporting the idea that the difference in the A/N ratio was due to a change in AMPAR-mediated currents.

To further investigate the subunit specificity of synaptic AMPAR incorporation, we focused on GluA1, a subunit of AMPARs that was previously shown to be delivered into synapses of layer 4–2/3, in the barrel cortex of 2-week-old animals (Takahashi et al. 2003). We overexpressed green fluorescent protein (GFP)-tagged GluA1 in layer 2/3 of the barrel cortex at P12, by Herpes simplex virus-mediated in vivo gene transfer. We subsequently prepared acute brain slices at P14 and examined synaptic responses at layer4–2/3 synapses of the barrel cortex by whole-cell recordings.

Overexpressed recombinant GFP-GluA1 forms homomeric receptors, which, in contrast to most endogenous AMPARs, are inwardly rectifying; that is, they display little outward current at positive membrane potentials compared with endogenous receptors. As was previously reported (Takahashi et al. 2003), GFP-GluA1-expressing neurons exhibited increased rectification compared with noninfected nearby neurons from intact whisker animals, but not from deprived whisker animals, indicating that whisker experience-dependent synaptic GFP-GluA1 delivery occurred (Fig 1*C*). In contrast, no difference in rectification at the synapses in layer 4–2/3 of the adult barrel cortex was seen after 2 days of GFP-GluA1 expression compared with nearby nonexpressing neurons, in either intact or whisker-deprived animals, indicating that there was no active synaptic delivery of GluA1 in the adult barrel cortex (Fig 1*D*). Thus, consistent with previous studies (Jitsuki et al. 2011; Wen and Barth 2011), we found that natural whisker experience does not drive AMPAR into barrel cortex synapses in adult animals.

Experience-Driven Synaptic AMPAR Delivery in the Barrel Cortex Persists in Adult NgR1-deficient Mice

We next examined whether NgR signaling is responsible for restricting the sensory experience-driven synaptic delivery of AMPAR in the adult barrel cortex. We first measured the A/N ratio at synapses onto layer 4–2/3 pyramidal neurons of the barrel cortex of NgR1-deficient P14 and 3-month-old mice. At P14, the A/N ratio was greater in intact than in whisker-deprived mutant mice (Fig 2*A*). In 3-month-old NgR1-deficient mice with intact whiskers, the A/N ratio was significantly greater than in mutant mice without whiskers or in WT mice with whiskers, indicating that the experience-driven synaptic AMPAR delivery persisted in the mutant adults (Figs 1*B* and 2*B*: A/N ratio of WT with whiskers, 1.417 ± 0.158, $n = 5$ animals; NgR1-deficient mice with whiskers, 1.903 ± 0.112, $n = 5$ animals; $P < 0.05$, Student's *t*-test). Notably, after only 2 days of whisker deprivation, the A/N ratio in 3-month-old NgR1-deficient mice decreased (Fig 2*B*), indicating that continuous AMPAR delivery is required to maintain the increased synaptic AMPAR content in adult NgR1-deficient mice. No increase in the A/N ratio was detected in the lateral pathway (between pyramidal neurons in layer 2/3) of the barrel cortex in 3-month-old NgR1-deficient mice versus WT mice, indicating that the synapses in layer 4–2/3 were selectively strengthened in the adult mutant mice (Fig 2*C*). No difference in the decay or input–output curve of the NMDAR-mediated synaptic

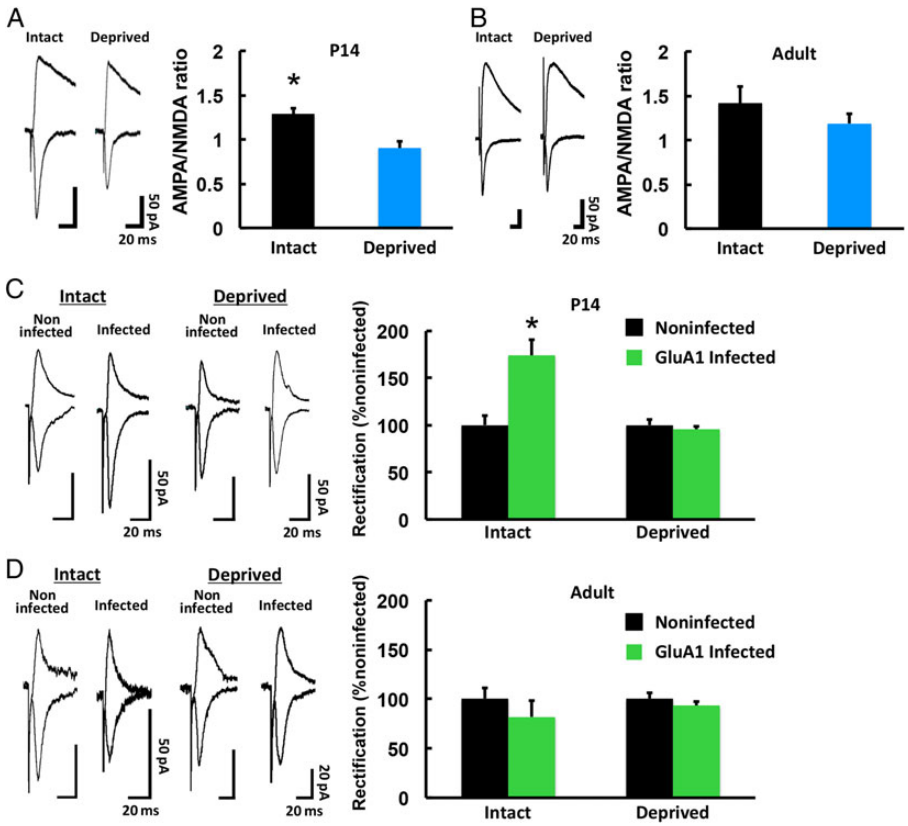

Figure 1. Experience-driven synaptic AMPAR delivery is limited in the adult barrel cortex. (A) (Left) Synaptic responses at layer 4–2/3 synapses in the barrel cortex of developing (P14) WT mice with (Intact) and without (Deprived) whiskers. Scale bars: 50 pA, 20 ms. (Right) Mean ratio of AMPAR-mediated currents to NMDA receptor-mediated currents (A/N ratio). Intact: $n = 5$ (11 cells from 5 animals); Deprived: $n = 5$ (10 cells from 5 animals). $^*P < 0.05$. (B) Synaptic responses at layer 4–2/3 synapses in the barrel cortex of adult (3-month-old) WT mice with (Intact) and without (Deprived) whiskers. Scale bars: 50 pA, 20 ms. (Right) Mean A/N ratio. Intact: $n = 6$ (17 cells from 6 animals); Deprived: $n = 5$ (13 cells from 5 animals). (C) (Left) Synaptic responses from neurons infected with Herpes simplex virus expressing GFP-GluA1 and from noninfected neurons (held at −60 mV and +40 mV, as indicated) at layer 4–2/3 synapses in the barrel cortex of P14 WT mice with (Intact) and without (Deprived) whiskers. The AMPAR-mediated responses were isolated by the application of 0.1 mM APV. Scale bars: 50 pA, 20 ms. (Right) Average rectification indices (RI; response at −60 mV/response at +40 mV) of neurons expressing GFP-GluA1 (green), normalized to the RI value of nearby noninfected cells (black). Intact: $n = 5$ (10 infected cells and 10 noninfected cells from 5 animals); Deprived: $n = 5$ (10 infected cells and 10 noninfected cells from 5 animals). $^*P < 0.05$. (D) (Left) Synaptic responses from neurons infected with Herpes simplex virus expressing GFP-GluA1 and from noninfected neurons at layer 4-2/3 synapses in the barrel cortex of adult WT mice with (Intact) and without (Deprived) whiskers. Scale bars: 20 pA, 20 ms. (Right) Average RI of neurons expressing GFP-GluA1 (green), normalized to the RI value of nearby noninfected cells (black). Intact: $n = 6$ (6 infected cells and 6 noninfected cells from 6 animals); Deprived: $n = 4$ (8 infected cells and 8 noninfected cells from 4 animals). Data were analyzed by Student's *t*-test. Data are presented as mean ± SEM.

responses was observed between intact and whisker-trimmed mutant P14 and adult mice (see Supplementary Fig 2), indicating that the A/N ratio reflected the synaptic AMPAR content.

We also overexpressed GFP-GluA1 in the barrel cortex of NgR1-deficient mice with intact whiskers at P12 or 3 months old (adult). After 2 days of expression, we detected increased rectification from the GFP-GluA1-expressing neurons compared with nearby noninfected neurons in both the 2-week-old and adult NgR1-deficient mice (Fig 2*D*,*E*), indicating that the experience-driven synaptic delivery of GluA1 occurred at both ages. However, we did not find any difference in rectification between GFP-GluA1-expressing and nearby nonexpressing neurons in the lateral pathway of the adult barrel cortex in the mutant mice (Fig 2*F*).

The paired-pulse ratio did not differ between WT and NgR1 mutant adult mice in the presence of whiskers (see Supplementary Figs 1*E* and 2*E*), indicating that there was no alteration in presynaptic release in the NgR1 mutant mice. Interestingly, however, while the paired-pulse ratio of WT mice did not differ between those with and without whiskers, the paired-pulse ratio of NgR1 mutant adult mice without whiskers was reduced compared with NgR1 mutant mice with whiskers and with WT mice. These observations indicate that presynaptic release is increased in adult NgR1 mutant mice without whiskers. This finding could be due to a homeostatic mechanism that compensates for the decreased postsynaptic function of adult NgR1 mutant mice in the absence of whiskers.

Taken together, these data indicate that NgR signaling limits sensory experience-driven synaptic AMPAR delivery in the adult barrel cortex.

NgR1's Effect on AMPAR Trafficking is Postsynaptic and Cell Autonomous

NgR1 is concentrated at postsynaptic densities in the adult cortex (Akbik et al. 2013). To examine whether the effect of NgR signaling on experience-driven synaptic AMPAR delivery is postsynaptic and cell autonomous, we cointroduced a fluorescent protein, Venus, with NgR1, into the barrel cortex of 3-month-old NgR1-deficient mice, using a Herpes virus vector with an internal ribosomal entry site (IRES). Two days later, NgR1-IRES-Venus-expressing neurons exhibited a significantly smaller A/N ratio than nonexpressing or Venus-only-expressing

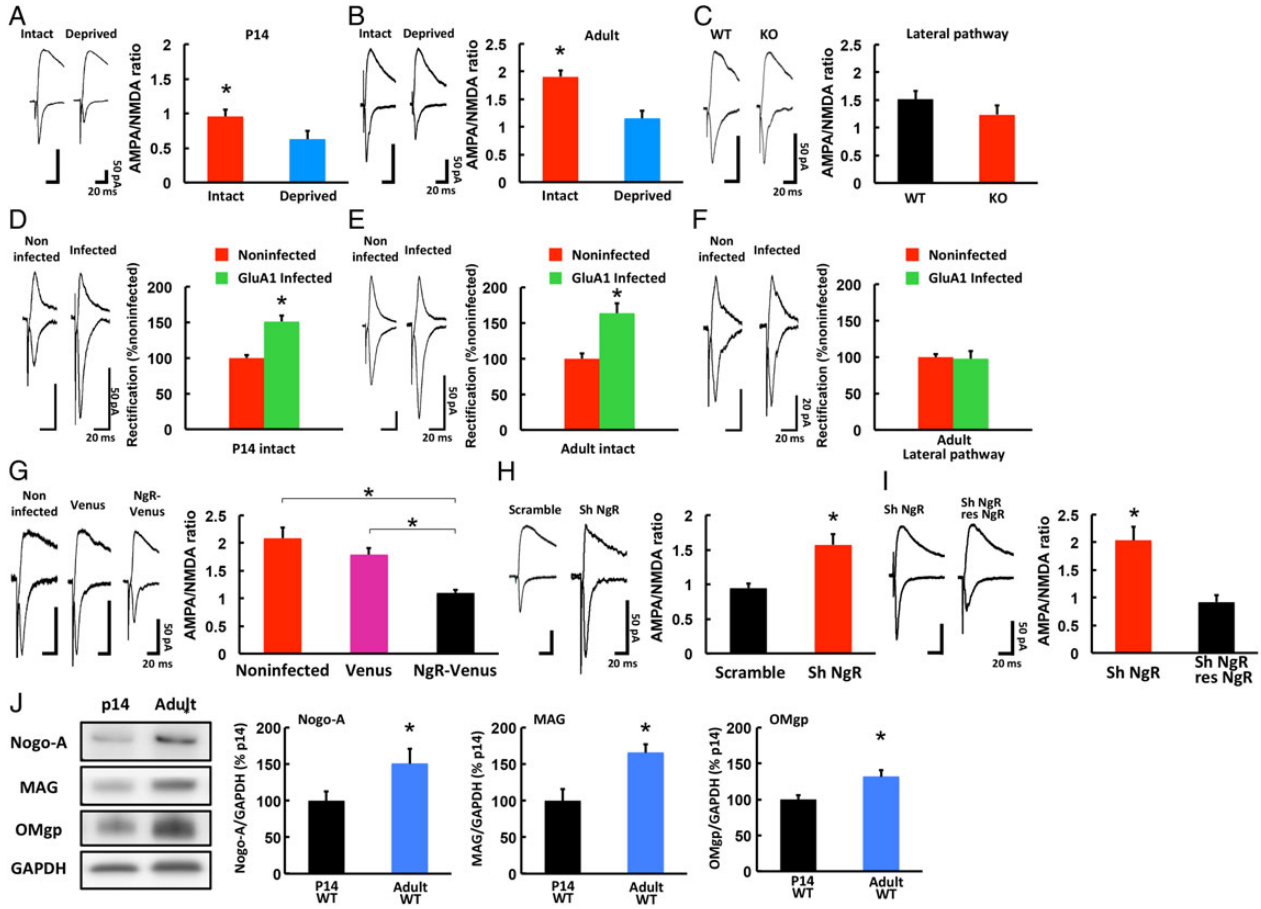

Figure 2. Experience-driven synaptic AMPAR delivery is restored in the adult barrel cortex of NgR1-deficient mice. (*A*) (Left) Synaptic responses at layer 4–2/3 synapses in the barrel cortex of developing (P14) NgR1-deficient mice with (Intact) and without (Deprived) whiskers. Scale bars: 50 pA, 20 ms. (Right) Mean A/N ratio. Intact: $n = 5$ (17 cells from 5 animals); Deprived: $n = 5$ (16 cells from 5 animals). $^*P < 0.05$. (*B*) (Left) Synaptic responses at layer 4–2/3 synapses in the barrel cortex of adult (3-month-old) NgR1-deficient mice with (Intact) and without (Deprived) whiskers. Scale bars: 50 pA, 20 ms. (Right) Mean A/N ratio. Intact: $n = 5$ (14 cells from 5 animals); Deprived: $n = 5$ (12 cells from 5 animals). $^*P < 0.05$. (*C*) (Left) Synaptic responses from layer 2/3 to layer 2/3 (lateral pathway) synapses in the barrel cortex of adult NgR1-deficient (KO) and WT mice. Scale bars: 50 pA, 20 ms. (Right) Mean A/N ratio. WT: $n = 6$ (15 cells from 6 animals); KO: $n = 5$ (11 cells from 5 animals). (*D*) (Left) Synaptic responses from neurons infected with Herpes simplex virus expressing GFP-GluA1 and from noninfected neurons (held at −60 mV and +40 mV, as indicated) at layer 4–2/3 synapses in the barrel cortex of P14 NgR1-deficient mice with intact whiskers (P14 intact). The AMPAR-mediated responses were isolated by 0.1 mM APV. Scale bars: 50 pA, 20 ms. (Right) Average rectification indices (RI; response at −60 mV/response at +40 mV) of neurons expressing GFP-GluA1 (green), normalized to the RI value of nearby noninfected cells (red). P14 Intact: $n = 5$ (11 infected cells and 11 noninfected cells from 5 animals). $^*P < 0.05$. (*E*) (Left) Synaptic responses from neurons infected with Herpes simplex virus expressing GFP-GluA1 and from noninfected neurons at layer 4–2/3 synapses in the barrel cortex of adult NgR1-deficient mice with intact whiskers (Adult intact). Scale bars: 50 pA, 20 ms. (Right) Average RI of neurons expressing GFP-GluA1 (green), normalized to the RI value of nearby noninfected cells (red). Adult intact: $n = 5$ (10 infected cells and 10 noninfected cells from 5 animals). $^*P < 0.05$. (*F*) (Left) Synaptic responses from layer 2/3 to layer 2/3 (lateral pathway) synapses infected with Herpes simplex virus expressing GFP-GluA1 and noninfected neurons in the barrel cortex of adult NgR1-deficient mice. Scale bars: 20 pA, 20 ms. (Right) Average RI of neurons expressing GFP-GluA1 (green), normalized to the RI value of nearby noninfected cells (red). Adult Lateral pathway: $n = 4$ (9 infected cells and 9 noninfected cells from 4 animals). (*G*) (Left) Synaptic responses from noninfected, Venus-expressing (Venus), and NgR1 IRES Venus expressing (NgR-Venus) neurons at layer 4–2/3 synapses in the barrel cortex of adult NgR1-deficient mice. Scale bars: 50 pA, 20 ms. (Right) Mean A/N ratio. Noninfected: $n = 4$ (12 cells from 4 animals), Venus: $n = 5$ (13 cells from 5 animals), NgR-Venus: $n = 4$ (8 cells from 4 animals). $^*P < 0.05$ Noninfected versus NgR-Venus and Venus versus NgR-Venus. (*H*) (Left) Synaptic responses from scrambled control-expressing (Scramble) and shNgR1-expressing (Sh NgR) neurons at layer 4–2/3 synapses of the WT adult barrel cortex. Scale bars: 50 pA, 20 ms. (Right) Mean A/N ratio. Scramble: $n = 5$ (10 cells from 5 animals); ShNgR1: $n = 5$ (11 cells from 5 animals). $^*P < 0.05$. (*I*) (Left) Synaptic responses from shNgR1-expressing (Sh NgR) and shNgR1+shRNA-resistant NgR1 (res-NgR) neurons at layer 4–2/3 synapses of the WT adult barrel cortex. Scale bars: 50 pA, 20 ms. (Right) Mean A/N ratio. ShNgR1: $n = 5$ (6 cells from 5 animals), ShNgR1+ res-NgR: $n = 5$ (6 cells from 5 animals). $^*P < 0.05$. (*J*) Expression level of Nogo-A, MAG, and OMgp in the synaptoneurosome fraction from P14 WT mice (p14 WT) and adult WT mice (Adult WT) mice. The GAPDH level was used as the reference in the quantitative analysis. The expression level of each protein in P14 WT mice was normalized to that in adult WT mice. p14 WT: $n = 6$; adult WT: $n = 6$. $^*P < 0.05$. Data were analyzed by Student's *t*-test (*A*, *B*, *C*, *D*, *E*, *F*, *H*, *I*, *J*) or one-way ANOVA followed by post hoc Bonferroni test (*G*). Data are presented as mean ± SEM.

neurons in NgR1-deficient mice, indicating that the postsynaptic expression of NgR1 rescued the effect of NgR1 loss on AMPAR trafficking (Fig 2*G*). Thus, the NgR signaling-induced prevention of experience-driven synaptic AMPAR incorporation is a postsynaptic and cell-autonomous effect.

To confirm this finding, we used short hairpin RNA (shRNA) to knock down the expression of endogenous NgR1. We introduced shNgR1 (detected by coexpressing GFP) into layer 2/3 of the barrel cortex of 3-month-old WT mice by lentivirus-mediated in vivo gene transfer. This NgR1 shRNA reduced the expression of endogenous NgR1 in primary cultures of cortical cells obtained from WT animals (see Supplementary Fig 2*F*). A week later, we prepared acute brain slices and recorded the synaptic transmission from pyramidal neurons in layer 4–2/3. The shNgR1-expressing neurons showed a higher A/N ratio than those expressing a scrambled control shRNA (Fig 2*H*).

We also tested whether the expression of shRNA-resistant NgR1 in NgR1 shRNA-expressing neurons would rescue the effect of the NgR1 shRNA expression on synaptic AMPAR content. We expressed NgR1 shRNA with shRNA-resistant NgR1-IRES-humanized Kusabira Orange1 (hKO1) in layer 2/3 pyramidal neurons of the WT adult barrel cortex, by lentivirus-mediated in vivo gene transfer. We found that the A/N ratio was rescued (i.e., decreased) in synapses onto pyramidal neurons expressing both NgR1 shRNA and shRNA-resistant NgR1 constructs, compared with nearby neurons expressing only the NgR1 shRNA construct (Fig 2*I*). These results support the interpretation that the NgR1 activation-induced prevention of synaptic AMPAR delivery is postsynaptic and cell autonomous, and they indicate that this finding was not due to a developmental defect.

Since NgR1 has several ligands, we also examined the expression levels of Nogo-A, OMgp, and MAG at P14 and in the adult. We found that the expression levels of all 3 ligands were increased in adult compared with P14 mice (Fig 2*J*). Since the increase of any one of these NgR1 ligands could restrict the delivery of synaptic AMPAR, the NgR1 deficiency might induce a more profound effect on synaptic AMPAR delivery than the knockout of any individual ligand.

LTP Induction is Facilitated in NgR1-Deficient Mice

The sustained experience-driven synaptic delivery of AMPAR in the adult barrel cortex of NgR1-deficient mice could be due to a lowered threshold for delivery. To examine this possibility, we induced long-term potentiation (LTP) in layer 4–2/3 synapses of the adult barrel cortex in WT or NgR1-deficient mice. We prepared acute brain slices from 3-month-old mice and performed whole-cell recordings, pairing 5 Hz stimulation (90 s) with postsynaptic depolarization at 0 mV. While this protocol failed to induce LTP in WT mice, LTP was induced in NgR1-deficient mice (Fig 3), indicating that synaptic plasticity is facilitated in the absence of NgR1.

NgR Functions with Coreceptor TROY to Prevent Experience-Driven Synaptic AMPAR Delivery

NgR has no transmembrane domain; thus, it activates intracellular signaling pathways via transmembrane coreceptors such as P75/TROY and Lingo-1 (Yiu and He 2006; Schwab 2010). Since Lingo-1 is largely expressed on axons (Lee et al. 2008), we focused on TROY as a potential mediator of the NgR signaling that prevents experience-driven synaptic AMPAR delivery. We examined whether knocking down TROY with shRNA (shTROY) would release the blockade of AMPAR delivery in adult WT mice, by expressing shTROY in layer 2/3 of the WT adult barrel cortex by lentivirus-mediated in vivo gene transfer. shTROY reduced the expression of endogenous TROY in primary cultures of cortical neurons from WT animals (see Supplementary Fig 3A).

A week later, we prepared acute brain slices and examined the synapses in layer 4–2/3. As with NgR1 knockdown, we detected a higher A/N ratio in the shTROY-expressing neurons than in those expressing the scrambled shRNA control construct (Fig 4A). Furthermore, we found that the A/N ratio of shTROY-expressing neurons was comparable to that of nonexpressing neurons in NgR1-deficient mice (Fig 4B), showing that the knockdown of TROY expression did not have an additive effect on the increase in synaptic AMPAR content in the absence of NgR1.

We also tested whether the expression of shRNA-resistant Troy in shTROY-expressing neurons would rescue the effect of shTROY expression on the synaptic AMPAR content. We expressed shTROY together with shRNA-resistant TROY-IRES-hKO1 in layer 2/3 pyramidal neurons of the WT adult barrel cortex, by lentivirus-mediated in vivo gene transfer. We found that the A/N ratio was rescued (i.e., decreased) in synapses onto pyramidal neurons expressing both shTROY and shRNA-resistant TROY constructs, compared with nearby neurons expressing only the shTROY construct (Fig 4C). Thus, TROY, a coreceptor of NgR, appears to prevent experience-driven synaptic AMPAR delivery in the adult barrel cortex, presumably by mediating NgR signaling.

ADF/cofilin Activation Mediates Experience-Driven Synaptic AMPAR Delivery in the Adult Barrel Cortex of NgR1-deficient Mice

NgR signaling is reported to regulate ADF/cofilin activity (Hsieh et al. 2006; Montani et al. 2009), which is directly linked to F-actin dynamics (Dillon and Goda 2005), and ADF/cofilin inactivation inhibits AMPAR trafficking (Gu et al. 2010). To examine whether ADF/cofilin activation mediates experience-driven synaptic AMPAR delivery in the adult barrel cortex of NgR1-deficient mice, we first examined the ADF/cofilin activity in the adult barrel cortex of mutant and WT animals. ADF/cofilin is inactivated by phosphorylation of its serine-3 (Ser3) residue, and activated by dephosphorylation. We therefore analyzed ADF/cofilin's Ser3 phosphorylation level in the adult barrel cortex of NgR1-deficient and WT mice. The ADF/cofilin showed lower phosphorylation on Ser3 in the mutant than in WT mice, indicating that its activity was higher in the mutant mice (Fig 4D).

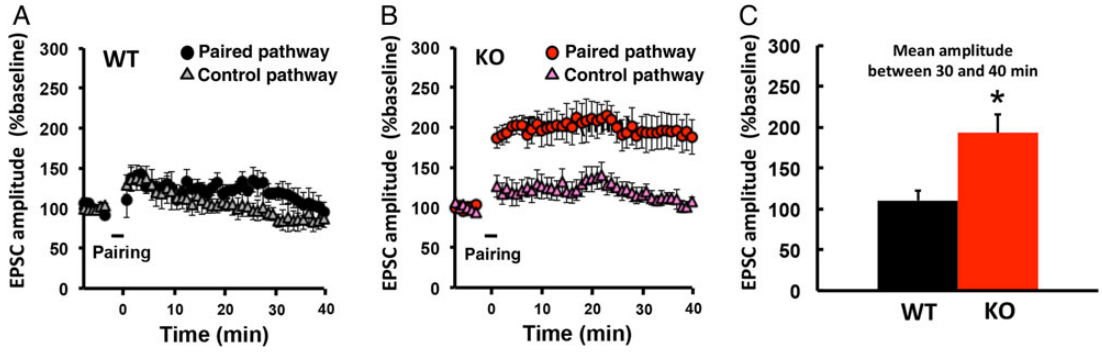

Figure 3. LTP induction is facilitated in adult NgR1-deficient mice. Acute brain slices were obtained from 3-month-old mice. Synaptic plasticity was induced by pairing 5 Hz stimulation (90 s) with postsynaptic potential at 0 mV in WT or NgR1-deficient (KO) mice. EPSC amplitude was normalized to the average baseline amplitude before pairing. (Right) Mean amplitude between 30 and 40 min after induction, normalized to the baseline amplitude. WT: $n = 5$ (5 cells from 5 animals); KO: $n = 6$ (6 cells from 6 animals). *$P < 0.05$. Data were analyzed by Student's *t*-test. Data are presented as mean ± SEM.

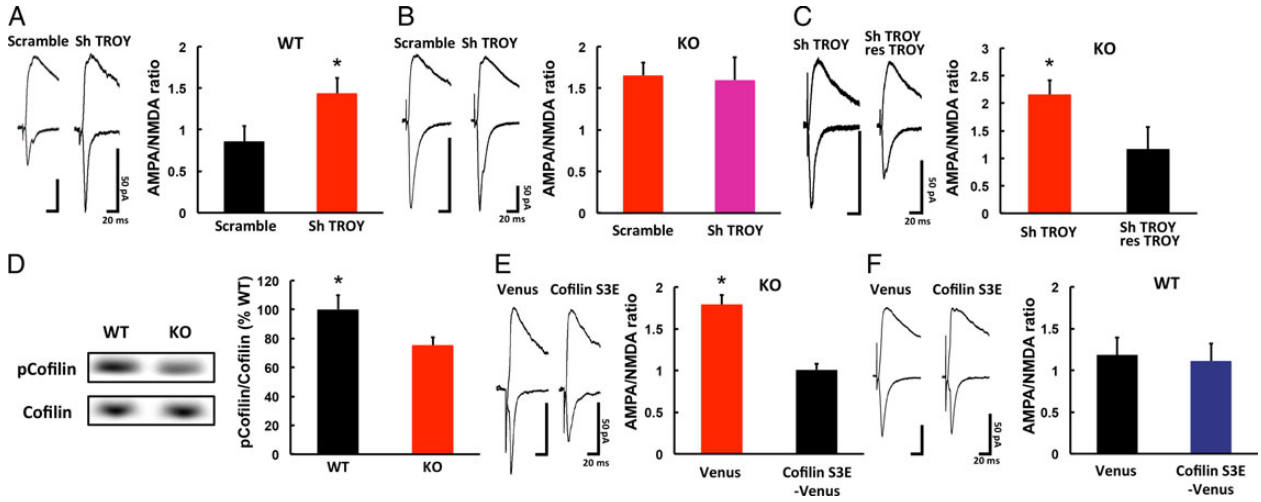

Figure 4. Signaling mechanism underlying the NgR1-mediated restriction of synaptic AMPAR delivery in the adult barrel cortex. (*A*) (Left) Synaptic responses from shTROY-expressing (Sh TROY) and scrambled control-shRNA-expressing (Scramble) neurons at layer 4–2/3 of WT adult barrel cortex. Scale bars: 50 pA, 20 ms. (Right) Mean A/N ratio. Scramble: $n = 5$ (10 cells from 5 animals); ShTROY: $n = 6$ (11 cells from 6 animals). $^*P < 0.05$. (*B*) (Left) Synaptic responses from shTROY-expressing (Sh TROY) and scrambled control-shRNA-expressing (Scramble) neurons at layer 4–2/3 synapses of NgR1-deficient adult barrel cortex. Scale bars: 50 pA, 20 ms. (Right) Mean A/N ratio. Scramble: $n = 5$ (10 cells from 5 animals); ShTROY: $n = 5$ (11 cells from 5 animals). (*C*) (Left) Synaptic responses from shTROY-expressing (Sh TROY) and shTROY+shRNA-resistant TROY (res-TROY) neurons at layer 4–2/3 synapses of the WT adult barrel cortex. Scale bars: 50 pA, 20 ms. (Right) Mean A/N ratio. ShTROY: $n = 5$ (6 cells from 5 animals), ShTROY+ res-TROY: $n = 5$ (6 cells from 5 animals). $^*P < 0.05$. (*D*) Phosphorylation level of ADF/cofilin in the synaptoneurosome fraction from the adult barrel cortex of WT and NgR1-deficient (KO) mice. The total ADF/cofilin level was used as the reference in the quantitative analysis. The ADF/cofilin phosphorylation level in KO mice was normalized to that of WT. WT: $n = 10$; KO: $n = 11$. $^*P < 0.05$. (*E*) (Left) Synaptic responses from Venus-tagged dominant-negative ADF/cofilin-expressing (Cofilin S3E-venus) and venus-expressing (Venus) neurons at layer 4-2/3 synapses of the NgR1-deficient adult barrel cortex. Scale bars: 50 pA, 20 ms. (Right) Mean A/N ratio. Cofilin S3E: $n = 4$ (9 cells from 4 animals); Venus: $n = 5$ (13 cells from 5 animals, same data in Fig. 2*G*). $^*P < 0.05$. (*F*) (Left) Synaptic responses from Venus-tagged dominant-negative ADF/cofilin-expressing (Cofilin S3E-venus) and venus-expressing (Venus) neurons at layer 4-2/3 synapses of the WT adult barrel cortex. Scale bars: 50 pA, 20 ms. (Right) Mean A/N ratio. Cofilin S3E: $n = 5$ (11 cells from 5 animals); Venus: $n = 5$ (9 cells from 5 animals). Data were analyzed by Student's *t*-test. Data are presented as mean ± SEM.

We next compared the amount of cofilin and phosphorylated cofilin between the crude lysate and the synaptoneurosome fraction. While the amount of phosphorylated cofilin in the synaptoneurosome fraction was comparable between WT and knockout mice, the total cofilin obtained from the synaptoneurosome fraction of NgR1-deficient mice was greater than that of WT mice (see Supplementary Fig 3*B*). This finding suggests that the relative amount of the active (nonphosphorylated on Ser3) form of cofilin in the synaptoneurosome fraction was greater in the NgR1-deficient mice than in the WT mice. Thus, the lack of NgR1 increases the relative amount of the active form of cofilin in the synaptoneurosome fraction.

Next, we coexpressed Venus and a dominant-negative ADF/cofilin mutant (Ser3 to glutamate: S3E) in the adult barrel cortex of NgR1-deficient mice, using a Herpes virus vector with an IRES. Two days later, we prepared acute brain slices and recorded synaptic transmission from layer 4–2/3. The A/N ratio was smaller in the ADF/cofilin S3E-IRES-Venus-expressing neurons than in those expressing Venus only (Fig 4*E*). The expression of ADF/cofilin S3E-IRES-Venus had no effect on the A/N ratio in WT mice (Fig 4*F*). These results suggested that the enhanced synaptic trafficking of AMPAR in the adult mutant mice involves the activation of ADF/cofilin.

Increased Surface Accumulation of AMPAR at Spines in Layer 2/3 of the Adult Barrel Cortex of NgR1-deficient Mice

Next, we examined the surface accumulation of AMPAR at spines in vivo, by live imaging with a 2-photon laser-scanning microscope. To acutely express recombinant genes, we used a Cre/loxP-mediated inducible expression system (Makino and Malinow 2011), in which Cre expression depends on 4-hydroxytamoxifen (4-OHT). Once Cre is expressed, it removes the floxed stop cassettes, inducing the expression of genes of interest. DNA constructs were delivered into layer 2/3 of the developing mutant and WT mouse barrel field by in utero electroporation (Fig 5*A*). GluA1 tagged with a pH-sensitive derivative of GFP (Super Ecliptic pHluorin, SEP) on the N-terminus (SEP-GluA1) was coexpressed with tdTomato in 2-month-old mice, by the intramuscular injection of 4-OHT. Two days after the injection, SEP-GluA1- and tdTomato-expressing neurons were observed in vivo, by the open skull method, with a two-photon microscope (Fig 5*A*,*B*). Whisker experience-dependent synaptic SEP-GluA1 delivery was observed in NgR1-deficient but not WT adult mice (see Supplementary Fig 4*A*,*B*), indicating that the 4-OHT-induced SEP-GluA1 behaved similarly to the GluA1 described above (Figs 1 and 2).

We measured the surface SEP-GluA1 at spines by normalizing the spine SEP signal to that of the nearby shaft area. The spine/dendrite ratio of SEP-GluA1 was higher in the NgR1-deficient than the WT mice in the presence of intact whiskers, indicating a greater enrichment of GluA1 on the spine surface of mutant compared with WT mice (Fig 5*C*,*D*). In the absence of whiskers (deprived for 2 or 3 days), the mutant mice exhibited a comparable spine/dendrite ratio of SEP-GluA1 to WT mice with intact whiskers, indicating that the increased surface trafficking of SEP-GluA1 at the spines of mutant mice is whisker experience-dependent (Fig 5*C*,*D*). We also found that a small fraction of spines exhibited an increased surface presentation of SEP-GluA1 in the adult barrel cortex of NgR1-deficient mice (Fig 5*E*). The spine size of NgR1-deficient mice with intact whiskers was comparable to those of WT mice with intact whiskers and mutant mice without whiskers, as

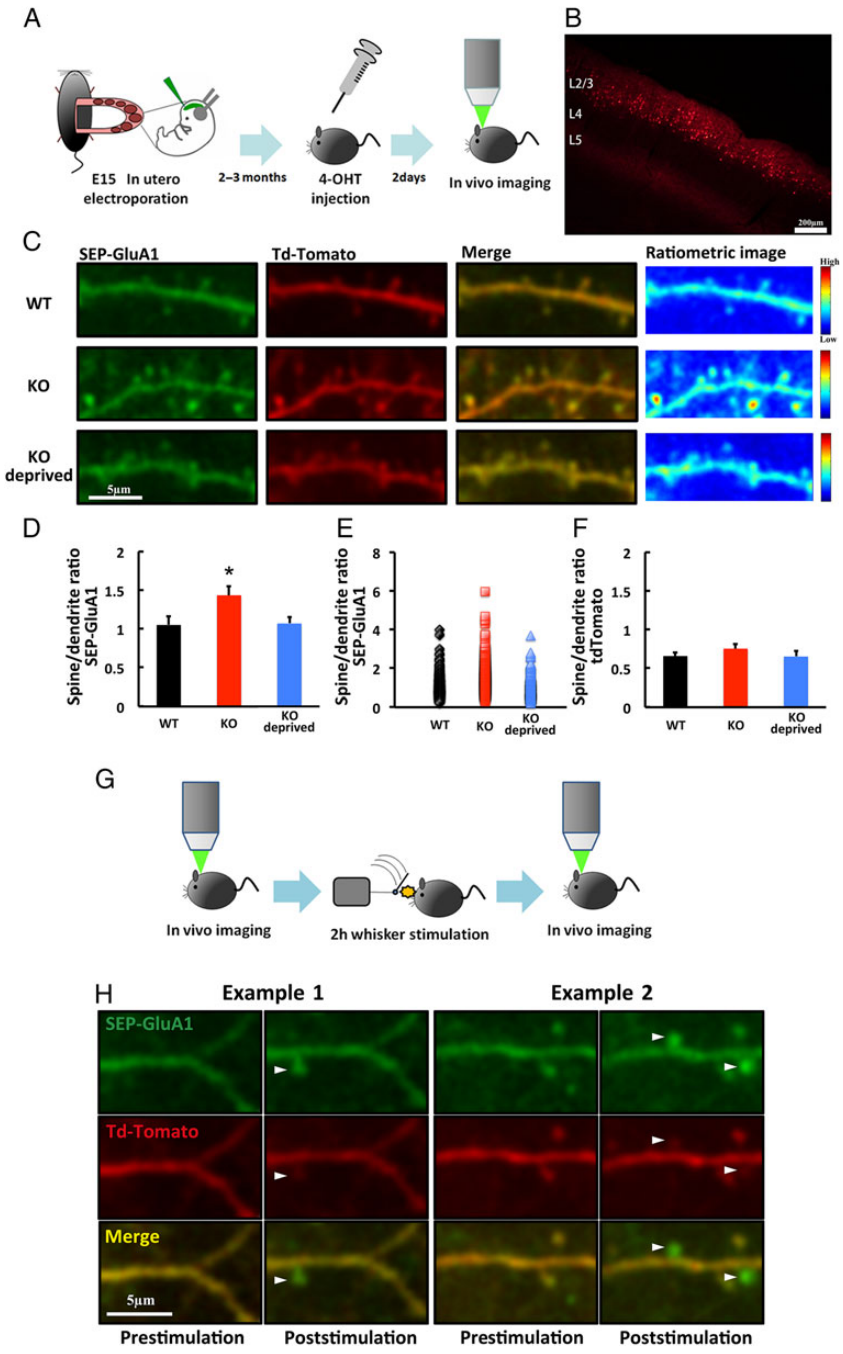

Figure 5. Surface accumulation of AMPAR is increased at spines in layer 2/3 of the adult barrel cortex of NgR1-deficient mice. (*A*) Schematic of the SEP-GluA1 and tdTomato expression and in vivo imaging. (*B*) Example of transfected neurons in layer 2/3 of the barrel cortex. Scale bar: 200 μm. (*C*) Examples of SEP-GluA1- and tdTomato-expressing neurons or pseudo-color ratiometric heat maps of the SEP-GluA1 intensity in adult WT mice and NgR1-deficient mice with (KO) and without (KO deprived) whiskers. Scale bar: 5 μm. (*D*) Ratio of fluorescence intensity in spines to dendritic shaft for SEP-GluA1 in adult WT mice and NgR1-deficient mice with (KO) and without (KO deprived) whiskers. WT: $n = 7$ (376 spines 7 animals); KO: $n = 7$ (403 spines from 7 animals); KO deprived: $n = 5$ (309 spines from 5 animals). $^*P < 0.05$ KO versus WT and KO versus KO deprived. (*E*) Scatter plot of spine-to-dendrite SEP-GluA1 ratios in adult WT mice and NgR1-deficient mice with (KO) and without (KO-deprived) whiskers. (*F*) Ratio of fluorescence intensity in spines to dendritic shaft for tdTomato in WT mice, and in NgR1-deficient adult mice with (KO) and without (KO deprived) whiskers. WT: $n = 7$ (376 spines 7 animals); KO: $n = 7$ (403 spines from 7 animals); KO deprived: $n = 5$ (309 spines from 5 animals). (*G*) Schematic of the in vivo imaging of animals with 2 h of whisker stimulation. (*H*) Examples of the surface accumulation of GluA1 on newly synthesized spines of adult NgR1-deficient mice after 2 h of whisker stimulation (arrowheads). Scale bar: 5 μm. Data in D, F were analyzed by one-way ANOVA followed by post hoc Fisher's Least Significant Difference (LSD). Data are presented as mean ± SEM. Representative images shown in the figures were Gaussian filtered.

determined by measuring the level of tdTomato (Fig 5*F*). Thus, the size of the spines did not contribute to the increased intensity of surface GluA1 in the NgR1-deficient mice compared with WT mice with intact whiskers and mutant mice without whiskers.

To assess the contribution of degradation on the alteration of GluA1 synaptic delivery, we examined the total protein level of GluA1 in the crude lysate of the adult barrel cortex from WT or NgR1-deficient mice and found no difference in the GluA1

expression level between them (see Supplementary Fig 4C). Furthermore, we detected no difference in the expression level of NEDD4, which ubiquitinates AMPARs (see Supplementary Fig 4D). In addition, no significant difference was seen in the ubiquitination level of GluA1 in the crude lysate between the mutant and WT adult barrel cortex (see Supplementary Fig 4E). These results suggest that the effect of degradation on the synaptic delivery of GluA1 was minimal. We also examined the phosphorylation levels of serine residues at 831 and 845 of GluA1 (Ser831, Ser845). The phosphorylation of Ser845 is thought to regulate the extrasynaptic membrane trafficking of GluA1 (Oh et al. 2006). Consistent with our in vivo imaging results, we detected an increased phosphorylation of Ser845 in the synaptoneurosome fraction obtained from the adult barrel cortex of NgR1-deficient mice compared with that of WT mice (see Supplementary Fig 4F). While we also found an increased phosphorylation of Ser831 in the synaptoneurosome fraction from the adult barrel cortex of NgR1-deficient mice compared with WT mice (see Supplementary Fig 4G), we detected no increase in CaMKII activity in the adult barrel cortex of mutant mice compared with WT mice (see Supplementary Fig 4H).

The upregulation of spine turnover in the adult barrel cortex of NgR1 mutant mice was recently reported (Akbik et al. 2013). To investigate the relationship between enhanced anatomical plasticity and synaptic function, we coexpressed SEP-GluA1 and tdTomato in layer 2/3 of the adult barrel cortex as described above, and observed the surface trafficking of AMPAR on layer 2/3 spines before and after 2 h of mechanical whisker stimulation (Fig 5G) (Jitsuki et al. 2011). We found a small number of newly synthesized spines after whisker stimulation in the NgR1-deficient but not the WT mice (KO: 9/275 spines/ 54 dendrites from 4 animals; WT: 0/293 spines /62 dendrites from 4 animals). Notably, surface SEP-GluA1 accumulated on the newly protruding spines of the mutant mice (Fig 5H). Although we could not conclude that 2 h of whisker stimulation produced a greater number of spines in the adult mutant barrel cortex than in the WT one, these results suggest that newly synthesized spines could contribute to the net increase in synaptic of AMPAR content in the adult brain of NgR1-deficient mice.

We also examined the spine morphology by Golgi staining. As was previously reported in the adult hippocampus (Lee et al. 2008), the number of mushroom-type mature spines was greater in the WT adult barrel cortex than in the NgR1-deficient cortex. Furthermore, the number of immature stubby-type spines was greater in the adult mutant barrel cortex than in that of WT (see Supplementary Fig 4I). Combined, the number of mushroom-type and stubby-type spines was comparable between the NgR1-deficient and WT mice (see Supplementary Fig 4I) as was the total number of spines (see Supplementary Fig 4I).

These data are consistent with the idea that Nogo signaling limits neural plasticity in the adult brain by restricting AMPAR trafficking in coordination with anatomical plasticity.

Discussion

Although some molecules have been identified as molecular "brakes" on experience-driven neural plasticity in the adult brain, the molecular and cellular mechanisms underlying this reduced plasticity have been unclear. Here we show that removing NgR1 releases a brake on adult neural plasticity by facilitating experience-driven synaptic AMPAR delivery. A recent study reported that the miniature EPSC amplitude in the developing hippocampus of triple NgR-deficient mice (NgR1-3 knockout mice) is slightly decreased, and the frequency is increased (Wills et al. 2012). Our finding that the A/N ratio in 2-weeks-old NgR1-deficient mice was slightly decreased compared with WT is consistent with their results (Figs 1A and 2A). In 2-week-old NgR1-deficient mice, the AMPAR removal from synapses might be higher in NgR1-deficient mice, and this could result in the slightly reduced synaptic AMPAR content in NgR1-deficient mice. Furthermore, these results suggest that NgR deficiency affects multiple brain areas.

Interestingly, only 2 days of whisker deprivation decreased the A/N ratio in 3-month-old NgR1-deficient mice (Fig 2B). This finding suggests that continuous AMPAR delivery is required to maintain the increased synaptic AMPAR content in adult NgR1-deficient mice. In addition, long-term depression (LTD)-like plasticity occurred in the adult barrel cortex in the absence of NgR1. Thus, both the delivery of AMPAR to synapses and its removal from synapses may be increased in the absence of NgR1, and the balance between these processes could determine the synaptic AMPAR content in NgR1-deficient mice.

Consistent with this interpretation, while spine turnover is increased, the total spine number is unchanged in the adult cortex and hippocampus of NgR1-deficient mice (see Supplementary Fig 4I) (Lee et al. 2008; Akbik et al. 2013). This finding also suggests that the increased AMPAR delivery in NgR1-deficient mice does not saturate the spines' ability to accommodate synaptic AMPAR, and LTP still can be induced. It is unclear if the mechanisms underlying the potential facilitation of LTD-like AMPAR removal from synapses are the same as in the enhancement of synaptic AMPAR content in NgR1-deficient mice. The activation of ADF/cofilin could increase actin dynamics and result in spine turnover. Such a mechanism could underlie both the increased incorporation and the removal of AMPARs from synapses.

We did not observe synaptic AMPAR delivery at the synapses in layer 4–2/3 in the barrel cortex of adult NgR1-deficient mice in the absence of whiskers (Fig 2). This observation suggests that synaptic AMPAR delivery in the adult barrel cortex of NgR1-deficient mice is not constitutive, but depends on the activity evoked by whisker deflection. When a whisker is deflected, the vertical pathway (layer 4–2/3), not the lateral pathway (layer 2/3 to layer 2/3), is most strongly activated by the principal whisker (Fox 2002; Feldman and Brecht 2005). Therefore, we think some activity threshold induces synaptic AMPAR delivery in the adult barrel cortex of NgR1-deficient mice, and the lateral pathway may not be activated strongly enough to drive AMPAR delivery (Fig 2F). Considering that ADF/cofilin was elevated in the adult barrel cortex of NgR1-deficient mice compared with WT mice, the upregulation of synaptic AMPAR delivery could have a widespread effect on synapses. Thus, the level of synaptic activity could determine the onset of synaptic AMPAR delivery.

As presented in Fig 5B, the spines we observed were a mixture of apical and basal dendritic spines. Furthermore, a previous paper reported the existence of apical dendritic spines that receive input from layer 4 (Shepherd et al. 2005). Consistent with these findings, we detected a number of spines with the SEP-GluA1 intensity from NgR1-deficient mice similar to that from WT animals, while some fractions of spines from mutant mice exhibited higher SEP-GluA1 signal than wild type (Fig 5E).

What is the mechanism for the NgR signaling-mediated prevention of synaptic AMPAR delivery? The postsynaptic knockdown of NgR1 or Troy in WT mice had the same effect on synaptic AMPAR levels (i.e., an increase) as was observed in NgR1-deficient mice (Figs 2H and 4A). The postsynaptic overexpression of NgR1 in the NgR1-deficient mice rescued the NgR1-deficient phenotype, leading to a decrease in synaptic AMPARs (Fig 2G). Nogo signaling is reported to upregulate the ADF/cofilin activity (Hsieh et al. 2006; Montani et al. 2009), which is directly

linked to F-actin dynamics (Dillon and Goda 2005), and ADF/cofilin inactivation inhibits AMPAR trafficking (Gu et al. 2010). However, we detected less ADF/cofilin activity in the adult barrel cortex of WT than NgR1-deficient mice (Fig 4*D*). We also found that the postsynaptic expression of dominant-negative ADF/cofilin prevented experience-driven synaptic AMPAR delivery in adult mutant mice (Fig 4*E*,*F*). The regulation of ADF/cofilin activity by NgR signaling could depend on the conditions and region of the nervous system. Thus, the postsynaptic inactivation of ADF/cofilin by NgR signaling may be responsible for restricting experience-driven synaptic AMPAR delivery in the adult cortex, and NgR1/Troy/cofilin signaling is likely to act at postsynaptic sites to restrict synaptic AMPAR delivery. We also found that the expression of dominant-negative ADF/cofilin did not have any effect on the synaptic AMPAR content in WT mice (Fig 4*F*). This finding suggests that the activation of ADF/cofilin is required for experience-driven synaptic AMPAR delivery, but not for basal experience-independent AMPAR recycling. Furthermore, a previous study reported that ERK1/2 activity is elevated in NgR1-deficient mice (Raiker et al. 2010). Since the activation of ERK1/2 facilitates synaptic AMPAR delivery (Qin et al. 2005), this could also contribute to the enhancement of synaptic AMPAR delivery in NgR1 mutant mice. NgR inhibits dendritic spine turnover (Akbik et al. 2013), which could result from the inactivation of ADF/cofilin. This inactivation could also contribute to the reduced synaptic AMPAR trafficking in the WT adult brain. The phosphorylation of Ser845 is considered to regulate extrasynaptic membrane trafficking of GluA1 (Oh et al. 2006). We detected increased phosphorylation of Ser845 in the synaptoneurosome fraction of the NgR1-deficient adult barrel cortex compared with WT (see Supplementary Fig 4*F*). This finding was consistent with our in vivo imaging results, which showed greater surface presentation of GluA1 on the spines of the mutant adult barrel cortex, compared with wild type.

We also detected greater phosphorylation on Ser831 in the synaptoneurosome fraction from the adult barrel cortex of NgR1-deficient than in WT mice (see Supplementary Fig 4*G*). Since we detected no differences in CaMKII activity in the adult barrel cortex of mutant and WT mice (see Supplementary Fig 4*H*), another kinase activity could be responsible for the increased phosphorylation on Ser831 in the mutant mice. The phosphorylation of Ser831 may regulate the synaptic insertion of GluA1 (Miyazaki, Takase, et al. 2012). Thus, both the extrasynaptic surface presentation of GluA1 and its lateral diffusion to synapses could be facilitated by the absence of NgR1.

Golgi staining revealed that the number of mushroom-type mature spines was greater in the WT adult barrel cortex than the NgR1-deficient one. Furthermore, more spines with immature morphology were present in the mutant mice. These results suggest that NgR1 signaling is required for the maturation of spines. The increased surface presentation of GluA1 should facilitate synaptic delivery, and it could be required for the establishment of stable synaptic connections. Thus, the surface presentation of GluA1 might be increased in immature spines to facilitate the establishment of stable synaptic connections, and this could be the reason why the surface presentation of GluA1 is increased in the NgR1-deficient adult barrel cortex than WT. Meanwhile, since the morphological analysis with STED (stimulated emission depletion) microscope is more sensitive than that with light microscopy, more careful examination will be required.

Removing the molecular brakes on adult plasticity is crucial for functional recovery from neurological injury. Our findings are useful for the therapeutic goal of repairing pathologic neural damage in adulthood.

Supplementary Material

Supplementary material can be found at http://www.cercor.oxfordjournals.org/ online.

Funding

This project was supported by Special Coordination Funds for Promoting Science and Technology from the Japan Science and Technology Agency (T.T.), "Development of biomarker candidates for social behavior" carried out under the Strategic Research Program for Brain Sciences by the Ministry of Education, Culture, Sports, Science and Technology (MEXT) of Japan (TT), and the Brain Mapping by Integrated Neurotechnologies for Disease Studies (Brain/Minds) carried out under the Strategic Research Program for Brain Sciences by the Ministry of Education, Culture, Sports, Science and Technology of Japan (T.T.), Innovative Areas "Neural Diversity and Neocortical Organization" of MEXT (SJ) and Takeda Science Foundation (SJ). Funding to pay the Open Access publication charges for this article was provided by Special Coordination Funds for Promoting Science and Technology.

Notes

We thank Drs Stephen Strittmatter for the NgR1-knockout mice and NgR1 construct, Roberto Malinow for the pCALNL-SEP-GluA1 and pCAG-ER^{T2}CreER^{T2} constructs, Michael Greenberg for the pLenti-Lox 3.7, pLenti-Lox 3.7-shNgR1, and pLenti-Lox 3.7-shTROY constructs, James Zheng for the cofilin S3E construct, and Hiroyuki Miyoshi and Atsushi Miyawaki for the IRES Venus construct. *Conflict of Interest*: None declared.

References

Akbik FV, Bhagat SM, Patel PR, Cafferty WB, Strittmatter SM. 2013. Anatomical plasticity of adult brain is titrated by Nogo Receptor 1. Neuron. 77:859–866.

Atwal JK, Pinkston-Gosse J, Syken J, Stawicki S, Wu Y, Shatz C, Tessier-Lavigne M. 2008. PirB is a functional receptor for myelin inhibitors of axonal regeneration. Science. 322:967–970.

Bavelier D, Levi DM, Li RW, Dan Y, Hensch TK. 2010. Removing brakes on adult brain plasticity: from molecular to behavioral interventions. J Neurosci. 30:14964–14971.

Bregman BS, Kunkel-Bagden E, Schnell L, Dai HN, Gao D, Schwab ME. 1995. Recovery from spinal cord injury mediated by antibodies to neurite growth inhibitors. Nature. 378:498–501.

Chen MS, Huber AB, van der Haar ME, Frank M, Schnell L, Spillmann AA, Christ F, Schwab ME. 2000. Nogo-A is a myelin-associated neurite outgrowth inhibitor and an antigen for monoclonal antibody IN-1. Nature. 403:434–439.

Clem RL, Barth A. 2006. Pathway-specific trafficking of native AMPARs by in vivo experience. Neuron. 49:663–670.

Dachtler J, Hardingham NR, Glazewski S, Wright NF, Blain EJ, Fox K. 2011. Experience-dependent plasticity acts via GluR1 and a novel neuronal nitric oxide synthase-dependent synaptic mechanism in adult cortex. J Neurosci. 31:11220–11230.

Dillon C, Goda Y. 2005. The actin cytoskeleton: integrating form and function at the synapse. Annu Rev Neurosci. 28:25–55.

Feldman DE. 2009. Synaptic mechanisms for plasticity in neocortex. Annu Rev Neurosci. 32:33–55.

Feldman DE, Brecht M. 2005. Map plasticity in somatosensory cortex. Science. 310:810–815.

Fournier AE, GrandPre T, Strittmatter SM. 2001. Identification of a receptor mediating Nogo-66 inhibition of axonal regeneration. Nature. 409:341–346.

Fox K. 2002. Anatomical pathways and molecular mechanisms for plasticity in the barrel cortex. Neuroscience. 111:799–814.

Franklin KBJ, Paxinos G. 2007. The mouse brain in stereotaxic coordinates third edition. New York (NY): Academic Press.

GrandPre T, Nakamura F, Vartanian T, Strittmatter SM. 2000. Identification of the Nogo inhibitor of axon regeneration as a Reticulon protein. Nature. 403:439–444.

Grutzendler J, Kasthuri N, Gan WB. 2002. Long-term dendritic spine stability in the adult cortex. Nature. 420:812–816.

Gu J, Lee CW, Fan Y, Komlos D, Tang X, Sun C, Yu K, Hartzell HC, Chen G, Bamburg JR, et al. 2010. ADF/cofilin-mediated actin dynamics regulate AMPA receptor trafficking during synaptic plasticity. Nat Neurosci. 13:1208–1215.

Harris KM, Jensen FE, Tsao B. 1992. Three-dimensional structure of dendritic spines and synapses in rat hippocampus (CA1) at postnatal day 15 and adult ages: implications for the maturation of synaptic physiology and long-term potentiation. J Neurosci. 12:2685–2705.

Hayashi Y, Shi SH, Esteban JA, Piccini A, Poncer JC, Malinow R. 2000. Driving AMPA receptors into synapses by LTP and CaMKII: requirement for GluR1 and PDZ domain interaction. Science. 287:2262–2267.

Holtmaat A, Svoboda K. 2009. Experience-dependent structural synaptic plasticity in the mammalian brain. Nature Rev Neurosci. 10:647–658.

Hsieh SH, Ferraro GB, Fournier AE. 2006. Myelin-associated inhibitors regulate cofilin phosphorylation and neuronal inhibition through LIM kinase and Slingshot phosphatase. J Neurosci. 26:1006–1015.

Issa NP, Trachtenberg JT, Chapman B, Zahs KR, Stryker MP. 1999. The critical period for ocular dominance plasticity in the Ferret's visual cortex. J Neurosci. 19:6965–6978.

Jitsuki S, Takemoto K, Kawasaki T, Tada H, Takahashi A, Becamel C, Sano A, Yuzaki M, Zukin RS, Ziff EB, et al. 2011. Serotonin mediates cross-modal reorganization of cortical circuits. Neuron. 69:780–792.

Kessels HW, Malinow R. 2009. Synaptic AMPA receptor plasticity and behavior. Neuron. 61:340–350.

Kim JE, Li S, GrandPre T, Qiu D, Strittmatter SM. 2003. Axon regeneration in young adult mice lacking Nogo-A/B. Neuron. 38:187–199.

Kim JE, Liu BP, Park JH, Strittmatter SM. 2004. Nogo-66 receptor prevents raphespinal and rubrospinal axon regeneration and limits functional recovery from spinal cord injury. Neuron. 44:439–451.

Lee H, Raiker SJ, Venkatesh K, Geary R, Robak LA, Zhang Y, Yeh HH, Shrager P, Giger RJ. 2008. Synaptic function for the Nogo-66 receptor NgR1: regulation of dendritic spine morphology and activity-dependent synaptic strength. J Neurosci. 28:2753–2765.

Lee HK, Takamiya K, Han JS, Man H, Kim CH, Rumbaugh G, Yu S, Ding L, He C, Petralia RS, et al. 2003. Phosphorylation of the AMPA receptor GluR1 subunit is required for synaptic plasticity and retention of spatial memory. Cell. 112:631–643.

Makino H, Malinow R. 2011. Compartmentalized versus global synaptic plasticity on dendrites controlled by experience. Neuron. 72:1001–1011.

Matsuo N, Reijmers L, Mayford M. 2008. Spine-type-specific recruitment of newly synthesized AMPA receptors with learning. Science. 319:1104–1107.

McGee AW, Yang Y, Fischer QS, Daw NW, Strittmatter SM. 2005. Experience-driven plasticity of visual cortex limited by myelin and Nogo receptor. Science. 309:2222–2226.

Mitsushima D, Ishihara K, Sano A, Kessels HW, Takahashi T. 2011. Contextual learning requires synaptic AMPA receptor delivery in the hippocampus. Proc Natl Acad Sci USA. 108:12503–12508.

Mitsushima D, Sano A, Takahashi T. 2013. A cholinergic trigger drives learning-induced plasticity at hippocampal synapses. Nat Commun. 4:2760.

Miyazaki T, Kunii M, Jitsuki S, Sano A, Kuroiwa Y, Takahashi T. 2013. Social isolation perturbs experience-driven synaptic glutamate receptor subunit 4 delivery in the developing rat barrel cortex. Eur J Neurosci. 37:1602–1609.

Miyazaki T, Kunii M, Tada H, Sano A, Kuroiwa Y, Goto T, Malinow R, Takahashi T. 2012. Developmental AMPA receptor subunit specificity during experience-driven synaptic plasticity in the rat barrel cortex. Brain Res. 1435:1–7.

Miyazaki T, Takase K, Nakajima W, Tada H, Ohya D, Sano A, Goto T, Hirase H, Malinow R, Takahashi T. 2012. Disrupted cortical function underlies behavior dysfunction due to social isolation. J Clin Invest. 122:2690–2701.

Montani L, Gerrits B, Gehrig P, Kempf A, Dimou L, Wollscheid B, Schwab ME. 2009. Neuronal Nogo-A modulates growth cone motility via Rho-GTP/LIMK1/cofilin in the unlesioned adult nervous system. J Biol Chem. 284:10793–10807.

Morishita H, Hensch TK. 2008. Critical period revisited: impact on vision. Curr Opin Neurobiol. 18:101–107.

Morishita H, Miwa JM, Heintz N, Hensch TK. 2010. Lynx1, a cholinergic brake, limits plasticity in adult visual cortex. Science. 330:1238–1240.

Oh MC, Derkach VA, Guire ES, Soderling TR. 2006. Extrasynaptic membrane trafficking regulated by GluR1 serine 845 phosphorylation primes AMPA receptors for long-term potentiation. J Biol Chem. 281:752–758.

Prinjha R, Moore SE, Vinson M, Blake S, Morrow R, Christie G, Michalovich D, Simmons DL, Walsh FS. 2000. Inhibitor of neurite outgrowth in humans. Nature. 403:383–384.

Qin Y, Zhu Y, Baumgart JP, Stornetta RL, Seidenman K, Mack V, van Aelst L, Zhu JJ. 2005. State-dependent Ras signaling and AMPA receptor trafficking. Genes Dev. 19:2000–2015.

Raiker SJ, Lee H, Baldwin KT, Duan Y, Shrager P, Giger RJ. 2010. Oligodendrocyte-myelin glycoprotein and Nogo negatively regulate activity-dependent synaptic plasticity. J Neurosci. 30:12432–12445.

Rumpel S, LeDoux J, Zador A, Malinow R. 2005. Postsynaptic receptor trafficking underlying a form of associative learning. Science. 308:83–88.

Ryu J, Futai K, Feliu M, Weinberg R, Sheng M. 2008. Constitutively active Rap2 transgenic mice display fewer dendritic spines, reduced extracellular signal-regulated kinase signaling, enhanced long-term depression, and impaired spatial learning and fear extinction. J Neurosci. 28:8178–8188.

Schwab ME. 2010. Functions of Nogo proteins and their receptors in the nervous system. Nat Rev Neurosci. 11:799–811.

Shepherd GM, Stepanyants A, Bureau I, Chklovskii D, Svoboda K. 2005. Geometric and functional organization of cortical circuits. Nat Neurosci. 8:782–790.

Shi S, Hayashi Y, Esteban JA, Malinow R. 2001. Subunit-specific rules governing AMPA receptor trafficking to synapses in hippocampal pyramidal neurons. Cell. 105:331–343.

Syken J, Grandpre T, Kanold PO, Shatz CJ. 2006. PirB restricts ocular-dominance plasticity in visual cortex. Science. 313:1795–1800.

Tada H, Kuroki Y, Funabashi T, Kamiya Y, Goto T, Suyama K, Sano A, Mitsushima D, Etgen AM, Takahashi T. 2013. Phasic synaptic incorporation of GluR2-lacking AMPA receptors at gonadotropin-releasing hormone neurons is involved in the generation of the luteinizing hormone surge in female rats. Neuroscience. 248:664–669.

Takahashi T, Svoboda K, Malinow R. 2003. Experience strengthening transmission by driving AMPA receptors into synapses. Science. 299:1585–1588.

Ungless MA, Whistler JL, Malenka RC, Bonci A. 2001. Single cocaine exposure in vivo induces long-term potentiation in dopamine neurons. Nature. 411:583–587.

Wen JA, Barth AL. 2011. Input-specific critical periods for experience-dependent plasticity in layer 2/3 pyramidal neurons. J Neurosci. 31:4456–4465.

Whitlock JR, Heynen AJ, Shuler MG, Bear MF. 2006. Learning induces long-term potentiation in the hippocampus. Science. 313:1093–1097.

Wills ZP, Mandel-Brehm C, Mardinly AR, McCord AE, Giger RJ, Greenberg ME. 2012. The nogo receptor family restricts synapse number in the developing hippocampus. Neuron. 73: 466–481.

Wright N, Glazewski S, Hardingham N, Phillips K, Pervolaraki E, Fox K. 2008. Laminar analysis of the role of GluR1 in experience-dependent and synaptic depression in barrel cortex. Nat Neurosci. 11:1140–1142.

Yiu G, He Z. 2006. Glial inhibition of CNS axon regeneration. Nat Rev Neurosci. 7:617–627.

Zamanillo D, Sprengel R, Hvalby O, Jensen V, Burnashev N, Rozov A, Kaiser KM, Koster HJ, Borchardt T, Worley P, et al. 1999. Importance of AMPA receptors for hippocampal synaptic plasticity but not for spatial learning. Science. 284:1805–1811.

Zheng B, Ho C, Li S, Keirstead H, Steward O, Tessier-Lavigne M. 2003. Lack of enhanced spinal regeneration in Nogo-deficient mice. Neuron. 38:213–224.